Chemical Physics Reviews

Negative inductor effects in nonlinear two-dimensional systems: Oscillatory neurons and memristors

Cite as: Chem. Phys. Rev. **3**, 041305 (2022); https://doi.org/10.1063/5.0124115
Submitted: 03 September 2022 • Accepted: 03 November 2022 • Published Online: 21 November 2022

Juan Bisquert

Chemical Physics Reviews REVIEW scitation.org/journal/cpr

Negative inductor effects in nonlinear two-dimensional systems: Oscillatory neurons and memristors

Cite as: Chem. Phys. Rev. 3, 041305 (2022); doi: 10.1063/5.0124115
Submitted: 3 September 2022 · Accepted: 3 November 2022 ·
Published Online: 21 November 2022

Juan Bisquert[a)]

AFFILIATIONS

Institute of Advanced Materials (INAM), Universitat Jaume I, 12006 Castelló, Spain

[a)]Author to whom correspondence should be addressed: bisquert@uji.es

ABSTRACT

Many chemical and physical systems show self-sustained oscillations that can be described by a set of nonlinear differential equations. The system enters oscillatory behavior by an intrinsic instability that leads to bifurcation. We analyze conducting systems that present oscillating response under application of external voltage or current. Phenomena like electrochemical corrosion and the spiking response of a biological neuron are well-known examples. These systems have applications in artificial neurons and synapses for neuromorphic computation. Their dynamical properties can be characterized by normal mode analysis of small expansion of the constituent nonlinear equations. The linearized model leads to the technique of ac frequency response impedance spectroscopy that can be obtained experimentally. We show a general description of two-variable systems formed by a combination of a fast variable (the voltage) and a slowing down internal variable, which produce a chemical inductor. A classification of bifurcations and stability is obtained in terms of the parameters of the intrinsic equivalent circuit including the case of a negative inductor. Thereafter, we describe a number of physical examples and establish the characterization of their properties: The electrocatalytic reaction with adsorbed intermediate species, an oscillating metal oxide memristor, and finally we discuss the signs of the equivalent circuit elements in the central model of neuroscience, the Hodgkin–Huxley model for an oscillating neuron.

TABLE OF CONTENTS

I. INTRODUCTION

Self-sustained oscillations is a general phenomenon associated with a breakdown of stability in nonlinear systems. Bifurcation by a change of external current or voltage provoking stationary oscillations is found in many natural and materials systems, such as neurons, memristors, and electrochemical devices.[1–3] An important tool for the analysis of these systems is the ac measurement of electrical characteristics by impedance spectroscopy,[4] and it has been well recognized the connection of oscillations by a Hopf bifurcation to the differential negative resistance, e.g., in electrocatalytic systems,[5–8] and in Mott memristors.[9] The analysis by impedance spectroscopy also shows the relevance across different disciplines[10–13] of the equivalent circuit model that contains a capacitor and a chemical inductor.[14]

The simplest approach to bifurcation in nonlinear systems consists of a two-dimensional system. It is generally believed that the occurrence of a Hopf bifurcation requires a separation of a fast destabilizing variable (u) and a slow stabilizing variable (x).[15] Here, "fast" and "slow" qualities are determined by the respective characteristic times τ that define the dynamics in the system of differential equation. When a nonlinear system of differential equations undergoes a Hopf bifurcation, there arises a limit cycle, which is a closed and isolated trajectory in the phase portrait $u \times x$. Models formed with the two essential oscillating variables find a wide range of applications.[1,16,17]

In a recent review, we classified the 2D dynamical systems showing bifurcation and oscillations using the methods of impedance spectroscopy and a collection of characteristic frequencies.[18] The work was based on the mentioned ordinary assumption that the destabilizing negative resistance occurs in the fast variable u. However, oscillatory behavior is possible in which the negative resistance occurs in the slow variable.[19] Here, we establish a more general classification framework that considers these different possibilities. We aim to find the sign of the equivalent circuit elements, as resistances and inductors, associated with instability and oscillations, since these elements can be obtained directly from impedance spectroscopy data. We elaborate a classification of systems in terms of the characteristic frequencies that can be obtained as products of the equivalent circuit elements. An important class of systems show a negative chemical inductor, and we examine the dynamical implications of this feature. We discuss a range of physical examples from material and natural systems in detail to show the properties of the framework of analysis and the presence of the negative inductor in physical systems. These methods have application in the construction of neuromorphic systems for building artificial intelligence closely coupled to perceptual systems.[20–25]

II. MODEL FOR 2D OSCILLATING SYSTEMS

We consider the general structure of a conduction–polarization system. The voltage across the device is u, and the current I_{tot} is affected by an internal process that contains a memory effect, represented by a state variable x that undergoes a slowing down response to the external perturbations. The system is described by the nonlinear coupled dynamical equations,

$$I_{tot} = C_m \frac{du}{dt} + \frac{1}{R_I} f(u,x), \tag{1}$$

$$\tau_k \frac{dx}{dt} = g(x,u). \tag{2}$$

The first equation is a conduction equation including the capacitive charging with capacitance C_m and a conduction channel of conductivity function $f(u,x)$ and resistance scale parameter R_I. Both R_I and C_m are considered positive constants. The fast characteristic time is henceforth

$$\tau_u = R_I C_m > 0. \tag{3}$$

Equation (2) describes the time evolution of the slowing variable x that responds to the changes by a voltage-driven adaptation function $g(x,u)$, with a characteristic time $\tau_k > 0$. The x may take a wide variety of interpretations according to the particular system: a concentration in chemical systems, such as electrocatalytic reactions, corrosion, and batteries; an ion channel current in neurons;[26] and an electronic current in semiconductors.[14]

There is a qualitative difference of Eqs. (1) and (2) in that only (1) includes the external current. We introduce the parameter

$$\varepsilon = \frac{\tau_u}{\tau_k}. \tag{4}$$

Normally, in the response to a perturbation, the charging of the capacitor is fast and the lower branch associated with the variable x is slower. Thus, the charging time constant τ_u is much shorter than the adaptation current time constant τ_k, hence $\varepsilon < 1$.

The stationary solution of Eqs. (1) and (2) is obtained by the null-clines $\dot{u} = 0$, $\dot{x} = 0$ that define the current–voltage curve $I_{tot}(u)$. An important resource for the better understanding of a nonlinear system is to develop a system of linear equations at a particular stationary point. This method is the foundation of the technique of impedance spectroscopy.[4,27,28] It is also a powerful tool to relate nonlinear models to linear data in electrical engineering, by the correspondence, for example, of transistor physics, nonlinear circuit theory, and a linear small perturbation equivalent circuit.[29,30] Therefore, to obtain insight into the properties of the dynamical systems (1) and (2), we consider the small signal expansion, where small perturbation quantities are denoted $\hat{y}$. We obtain

$$\hat{I}_{tot} = C_m \frac{d\hat{u}}{dt} + \frac{1}{R_b}\hat{u} + \frac{f_x}{R_I}\hat{x}, \tag{5}$$

$$\tau_k \frac{d\hat{x}}{dt} = g_u \hat{u} + g_x \hat{x}, \tag{6}$$

where

$$R_b = \frac{R_I}{f_u}. \tag{7}$$

We observe in Eq. (5) that the conduction equation of Eq. (1) is divided in three parallel branches. We have described previously the impedance model of Eqs. (5) and (6) with respect to the angular frequency ω.[14,18] [Note that the f function in (1) and (5) has the opposite sign in Ref. 18.] We take the Laplace transform of Eqs. (5) and (6), $d/dt \to s$, where $s = i\omega$, and we arrive at

$$Z(s) = \frac{\hat{u}}{\hat{I}_{tot}} = \left[C_m s + {R_b}^{-1} + \frac{1}{R_a + L_a s} \right]^{-1}. \tag{8}$$

The circuit elements are defined as

$$R_a = -\frac{R_I g_x}{f_x g_u}, \tag{9}$$

$$L_a = \frac{R_I \tau_k}{f_x g_u}, \tag{10}$$

and the equivalent circuit contains the capacitor, two resistances, and inductor as shown in Fig. 1. This is the circuit associated with the chemical inductor model characterized in recent publications.[14,31] As shown previously in general terms, the model of Eqs. (1) and (2) always gives the (R_a, L_a) branch that forms a chemical inductor.[14] We have the inductor time constant,

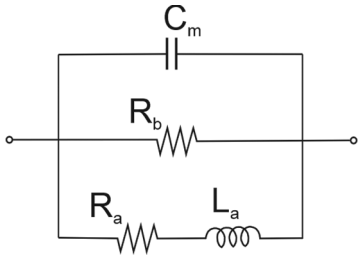

FIG. 1. Equivalent circuit model.

$$\tau_L = \frac{L_a}{R_a} = -\frac{\tau_k}{g_x}. \tag{11}$$

Alternatively, we use the characteristic frequency

$$\omega_L = \frac{R_a}{L_a} = -\frac{g_x}{\tau_k}. \tag{12}$$

The total differential resistance of Eq. (8) is

$$R_{dc}^{-1} = \frac{1}{R_b} + \frac{1}{R_a}. \tag{13}$$

III. INTERPRETATION OF FAST–SLOW CONDUCTING SYSTEMS

The model posed in Eqs. (1) and (2) is fairly broad, and it covers a large variety of systems. Let us discuss the interpretation of the physical behavior that is represented by such class of models. In this section, we consider the dynamic properties when the system operates in a stable domain, in order to clarify the meaning of the equivalent circuit approach.

For clarity, we consider the particular systems of the type $f(u,x) = \phi_c(u) + R_I x$, in which Eq. (1) becomes

$$I_{tot} = C_m \frac{du}{dt} + \frac{1}{R_I}\phi_c(u) + x. \tag{14}$$

Clearly, x has the meaning of a current. The total current I_{tot} in Eq. (14) is thus split in three components. These components act differently when a voltage pulse is applied. The capacitive current and the conduction current ϕ_c/R_I are set rapidly as shown in Fig. 2(a). (In practice there is a charging time controlled by a series resistance but we ignore such a feature for simplicity.[25]) In contrast, the current x of the "slow mode" lags behind by the time τ_k, since it requires a relaxation process determined by Eq. (2). At longer time, the initial capacitive current vanishes and the total current is $\phi_c/R_I + x$, as shown in Fig. 2(b). Such an increase in current is the central property of the chemical inductor, which implies a decrease in the total resistance at long time.[31]

Figure 2 has provided a clear interpretation of those particular systems indicated in Eq. (14) in which the system decouples the conduction current in two separate components, fast and slow. Still the problem is highly nonlinear in the functions $\phi_c(u)$ and $g(u,x)$. However, the general form of Eq. (1) provides a broad variety of cases that are not decoupled, for example the slow variable can be a surface voltage instead of current,[32] or the function $f(u,x)$ may be highly convoluted, as in the memristor model described here in Sec. IX.

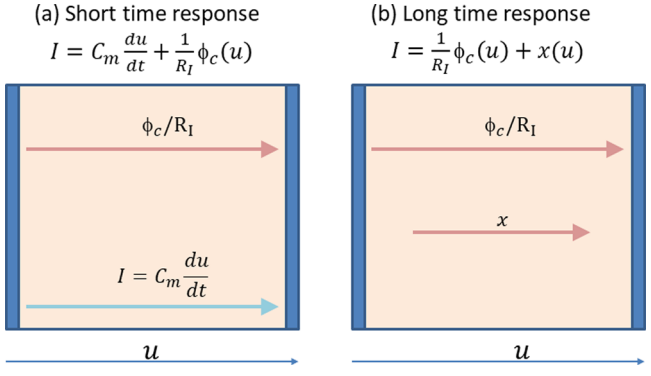

FIG. 2. Schematic view of current in a conducting fast–slow system where $f(u,x) = f_c(u) + R_I x$: (a) short and (b) long time response.

Even though the full nonlinear system may very rather involved, we have noticed in (5) that the small perturbation procedure always produces a separation of the currents into the components in $\hat{u}$ and $\hat{x}$. This enables us to visualize the different components of the current as in Fig. 2, as represented in the equivalent circuit in Fig. 1, which is generally valid for any class of coupling. Many examples and insights to this equivalent circuit model have been presented recently.[14,33]

We now discuss the dynamical properties in the frequency domain, determined by the impedance function (8). In Fig. 3(a), we show the characteristic spectrum that is obtained in a stable regime, further discussed in Sec. IV. We observe in Fig. 3 that the different dynamic regimes of Fig. 2 provide distinct spectral features in the complex plane representation of the impedance. At high frequency, the (R_b, C_m) elements produce a typical arc with associated resistance R_b, Fig. 3(b). At lower frequencies, the inductor impedance is reduced and the additional parallel resistance R_a becomes relevant, reducing the total resistance to the value R_{dc} of Eq. (13) and producing the negative arc in the fourth quadrant, Fig. 3(c), characteristic of the chemical inductor.

IV. DIVERGENCE OF THE SLOW VARIABLE

We have discussed previously that 2D models for self-sustained oscillating systems, such as neurons, require a negative differential resistance (NDR) that destabilizes the system.[18] In many cases, the negative resistance occurs from the fast u-branch of the model, i.e., the function f_u gives a negative R_b in Eq. (7), while the total resistance R_{dc} is positive. One example of this structure is the FitzHugh–Nagumo (FHN) neuron equations that has been broadly studied by its rich phase portraits.[1,34–36] It is defined by the functions[37]

$$f = \frac{u^3}{3} - u + R_I x, \tag{15}$$

$$g = \frac{r}{R_I}u - bx, \tag{16}$$

with three positive parameters, ε, r, and b. Applying Eqs. (7)–(10) to this model, we obtain the equivalent circuit elements of row 5 of Table I, and the dc resistance is

$$R_{dc} = R_I\left[u^2 - 1 + \frac{r}{b}\right]^{-1}. \tag{17}$$

The properties and behavior of the model are illustrated in Fig. 4 and discussed in Sec. VI. The NDR that destabilizes the system occurs in R_b for $|u| < 1$, as mentioned earlier.

In general, the sign of g_x takes special general significance for the dynamical properties. It determines the sign of the inductor time constant $\omega_L = 1/\tau_L$, which becomes negative if $g_x > 0$ by Eqs. (11) and (12). Numerous examples of 2D dynamical systems with oscillating structure in which $g_x < 0$ have been reviewed.[18] This is the case for FHN model in Eqs. (15) and (16), in which $g_x = -b < 0$ so that the slow variable stabilizes the system. This mechanism

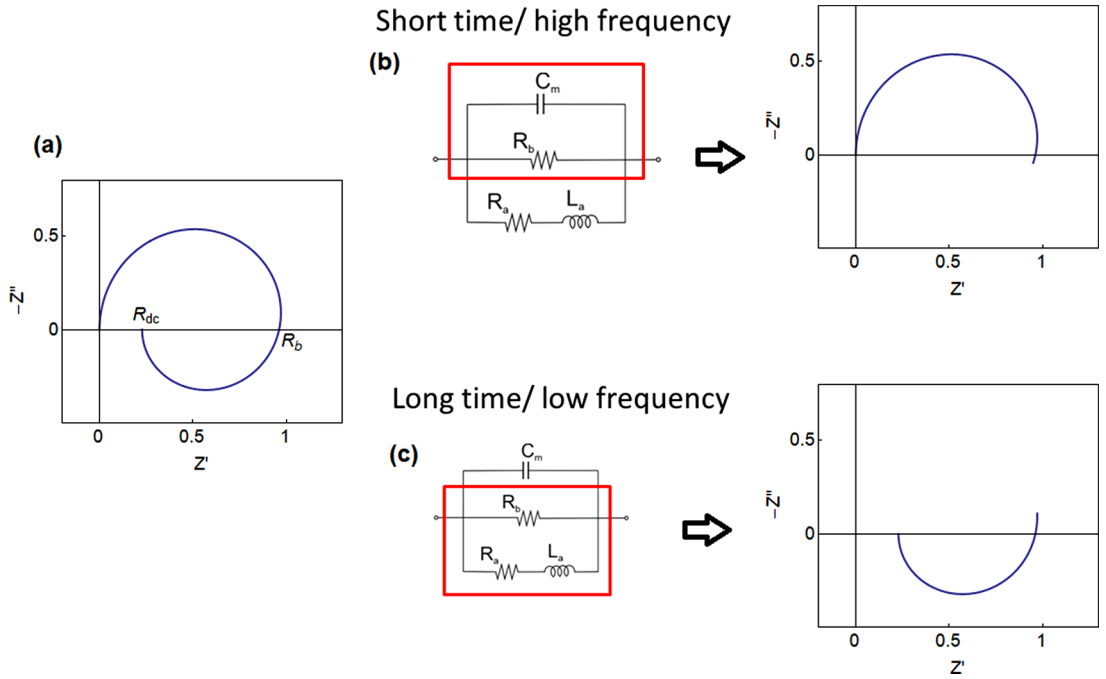

FIG. 3. (a) Characteristic impedance spectrum of the model of Fig. 1. (b) High-frequency part of the spectrum. (c) Low-frequency part of the spectrum, and the correspondent active fragments of the equivalent circuit.

is rather common in the analysis of systems with self-sustained oscillations.

For a broader analysis, consider a small perturbation of voltage Δu. Integrating Eq. (6), we have[4,7]

$$x = \frac{g_u}{g_x}|\Delta u|(1 - e^{-t/\tau_L}). \tag{18}$$

For $g_x > 0$ and $\omega_L = 1/\tau_L < 0$, this equation indicates a possible instability in which x grows indefinitely. The negative time element occurs now in the a-branch, and it can be caused by the resistance R_a or by the inductor L_a. However, the negative time constant feature competes with the stabilizing effect of the fast variable. A complete normal mode analysis will be presented below.

According to these different possibilities, of having negative elements either in channel a or b, we present here a more general analysis adapted to the signs of the partial derivates of the functions f, g. More concretely, the circuit elements are determined by the signs of g_x, as already mentioned, and by the sign of the product $f_x g_u$. The resulting properties of the circuit elements are shown in Table I, rows 1–4. We obtain that R_a and L_a can be either positive or negative, depending of the combination of signs. There are two situations that avoid the exponential explosion, corresponding to $g_x < 0$, if both R_a and L_a are positive or if both are negative.

TABLE I. Signs and values of the circuit elements and time constant.

	g_x	$f_x g_u$	f_u	R_b	R_a	L_a	$\tau_L = L_a/R_a$
				$\frac{R_I}{f_u}$	$-\frac{R_I g_x}{f_x g_u}$	$\frac{R_I \tau_k}{f_x g_u}$	$-\tau_k/g_x$
1	−	+			+	+	+
2	−	−			−	−	+
3	+	+			−	+	−
4	+	−			+	−	−
5-FHN	$-b$	r	$u^2 - 1$	$\frac{R_I}{u^2-1}$	$\frac{b}{r}R_I$	$\frac{\tau_k}{r}R_I$	$\frac{\tau_k}{b}$
6	β	r	$a + u$	$\frac{R_I}{a+u}$	$-\frac{\beta}{r}R_I$	$\frac{\tau_k}{r}R_I$	$-\frac{\tau_k}{\beta}$
7-diffusive memristor	F'	$\frac{R_I}{R_\delta}$	$\frac{1}{\cosh\left(\frac{x}{\delta}\right)}$	$R_I \cosh\left(\frac{x}{\delta}\right)$	$-R_\delta F'$	$R_\delta \tau_k$	$-\frac{\tau_k}{F'}$

V. STABILITY AND BIFURCATION IN 2D SYSTEMS

For a general analysis of the stability properties, we obtain the Jacobian of Eqs. (5) and (6) that can be written as follows:

$$\begin{pmatrix} -\frac{f_u}{\tau_u} & -\frac{f_x}{\tau_u} \\ \frac{g_u}{\tau_k} & \frac{g_x}{\tau_k} \end{pmatrix}. \tag{19}$$

The determinant has the expression

$$\Delta = \frac{f_x g_u - f_u g_x}{\tau_u \tau_x}. \tag{20}$$

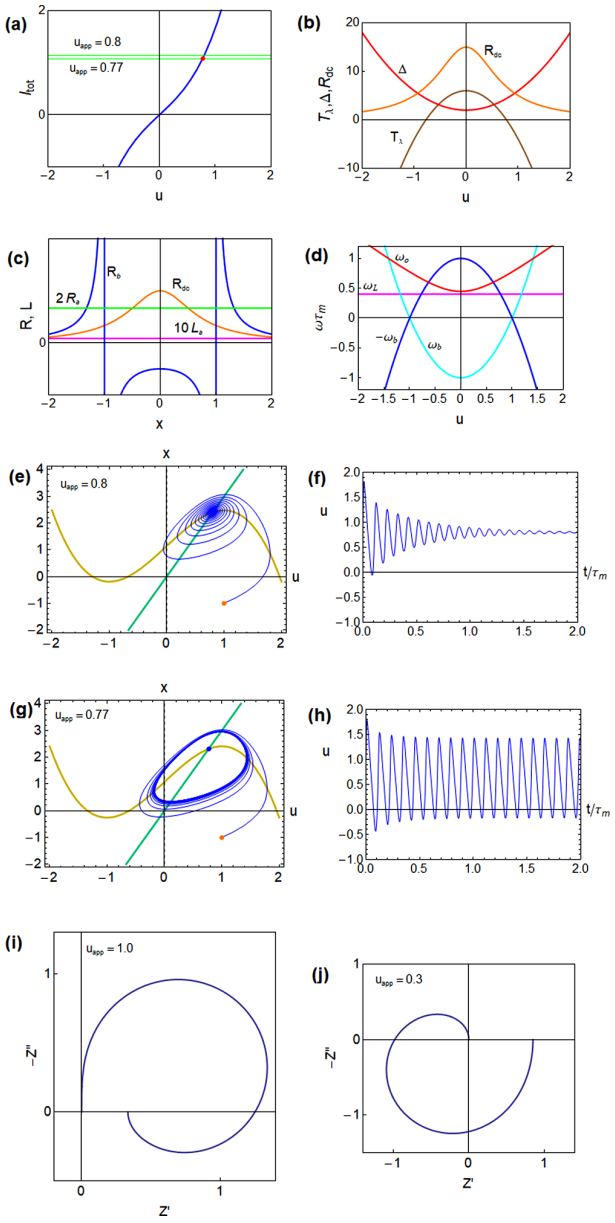

FIG. 4. Dynamical properties in a realization of FHN model: (a) current–voltage curve. The green lines are the current obtained at selected voltages expanded in (e) and (g). The red point is the Hopf bifurcation at positive voltage. (b) Stability variables. The red points are Hopf bifurcations. (c) Circuit elements. (d) Characteristic frequencies. [(e) and (g)] Nullclines and trajectory in phase space. The *f*-nullcline is the yellow line, and *g*-nullcline is the green line. The orange point is the starting condition. [(f) and (h)] Voltage evolution with time. [(i) and (j)] Impedance spectra. Parameters: $R_l = 0.5$; $b = 0.8$; $r = 1.2$; $\epsilon = 0.5$, $\tau_m = 0.01$.

By comparing Eq. (13), we obtain the equation that relates the determinant to the dc resistance,

$$\Delta = -\frac{g_x}{\tau_k C_m}\frac{1}{R_{dc}}. \tag{21}$$

The first stability condition is $\Delta > 0$. Only if $g_x < 0$, the sign of the total differential resistance and the sign of the determinant coincide. Therefore, when the system is destabilized by x (corresponding to $g_x > 0$), the total resistance can be negative in situations of stability, and vice versa. We will see examples later on.

The trace of the matrix (18) is

$$T_\lambda = -\frac{f_u}{\tau_u} + \frac{g_x}{\tau_k}. \tag{22}$$

For $\Delta > 0$ and $T_\lambda > 0$, the fixed point becomes an unstable source and generates a limit cycle trajectory. The Hopf bifurcation is determined by the condition $T_\lambda = 0$. It can be written as follows:

$$f_u = \frac{\tau_u}{\tau_k} g_x. \tag{23}$$

Alternatively

$$R_b C_m = -\tau_L = -\frac{L_a}{R_a}. \tag{24}$$

There are two situations in which the oscillations occur. First, if the destabilizing variable is the fast one, then $g_x < 0$, as explained in Table I, and the oscillations require a negative component in f_u, i.e., a negative R_b. This is a typical situation, and many examples have been presented in a previous review.[18]

On the other hand, if $g_x > 0$ the system can oscillate with the R_b resistance remaining positive. This situation is associated with negative inductor L_a or negative R_a and is the main topic of this paper. Several examples will be discussed in Secs. VII–X.

VI. ANALYSIS OF STABILITY BY IMPEDANCE SPECTROSCOPY

For the analysis of conducting/oscillating systems by impedance spectroscopy, it is very useful to relate spectral shapes to the inherent dynamical properties.[15,38–40] We showed recently that the impedance patterns can be classified by a series of characteristic frequencies that are introduced in Table II.[18]

In this paper, we restrict the analysis to condition of constant current. In galvanostatic operation, the Hopf bifurcations are given by the poles of the impedance, i.e., the zeros of the admittance $Y = Z^{-1}$ at a

TABLE II. Characteristic frequencies.

ω_a		$-\frac{1}{\tau_u}\frac{f_x g_u}{g_x}$	$\frac{1}{R_a C_m}$	$-\frac{1}{R_\delta C_m F'}$
ω_b		$\frac{f_u}{\tau_u}$	$\frac{1}{R_b C_m}$	$\frac{1}{\tau_u \cosh\left(\frac{x}{\delta}\right)}$
$-\omega_b$				
ω_L		$-\frac{g_x}{\tau_k}$	$\frac{R_a}{L_a} = \frac{1}{\tau_L}$	$-\frac{F'}{\tau_k}$
Δ		$\frac{1}{\tau_u \tau_k}(f_x g_u - f_u g_x)$	$\omega_L(\omega_a + \omega_b)$	
ω_o		$\Delta^{1/2}$	$[\omega_L(\omega_a + \omega_b)]^{1/2}$	
T_λ		$-\frac{f_u}{\tau_u} + \frac{g_x}{\tau_k}$	$-\omega_b - \omega_L$	

finite frequency.[2] The oscillations at fixed voltage require a series resistance that introduces additional complexity.[18]

The poles of the impedance correspond to the condition of imaginary eigenvalues $\lambda = i\omega_o$ that determines the Hopf bifurcation.[41,42] The condition can be written as follows:

$$\omega_L = -\omega_b. \tag{25}$$

This expression is complementary to those provided above in Eqs. (23) and (24).

As a reference, we revise the properties of the FHN model, shown in Fig. 4, that have been described before.[18,37] Figure 4(b) shows that the dc resistance is positive, as the $I-u$ curve in Fig. 2(a) does not have a negative characteristic. Figures 4(b) and 4(c) show that R_a and L_a are positive, while the negative R_b in Fig. 4(c) produces a region of $T_\lambda > 0$ in which limit cycle oscillations occur, as shown in Figs. 4(g) and 4(h). For higher voltage, the system arrives to a fixed point, Figs. 4(e) and 4(f). Figure 4(d) shows the condition for the Hopf bifurcation, given by the intercept of ω_L and $-\omega_b$ by Eq. (25). Figure 4(i) shows the impedance pattern associated with the chemical inductor structure[14] in the stable region of voltage, same as Fig. 3(a). This impedance is quite universal and it has been measured in a variety of conducting systems as neurons,[43] electrochemistry,[10–13] and solar cells.[44] The impedance pattern associated with limit cycle oscillations shown in Fig. 4(j) displays a negative resistance at intermediate frequencies.[2,18]

VII. NEGATIVE INDUCTOR

As mentioned before, it is interesting to discuss the sign of the equivalent circuit elements and their implications for stability and bifurcation. The effect of the sign of R_b is well known, as in the FHN model described in Fig. 4. Let us focus on the elements of the inductor line in the equivalent circuit of Fig. 1.

Consider the following model in that we introduce for the purpose of illustration:

$$f = au + \frac{u^2}{2} + R_I x, \tag{26}$$

$$g = \frac{r}{R_I}u + \beta x. \tag{27}$$

The parameters of the model are r, β, ϵ, a, and the equivalent circuit elements are given in row 6 of Table I.

The model is similar to FHN but with a linear R_b. The parameters a, r, and β can take both positive and negative sign. The resulting sign of the equivalent circuit elements is indicated in Table III. The first line in Table III coincides with the signs of FHN. Here, we focus in the alternative stable structure given by the line 2 of Table III. The dynamical properties of this situation are shown in detail in Fig. 5.

TABLE III. Sign of equivalent circuit elements.

	r	β	R_a	L_a	ω_L
FHN	+	−	+	+	+
2	−	−	−	−	+
3	+	+	−	+	−
4	−	+	+	−	−

The model has a region of negative resistance R_{dc} that coincides with the negative values of Δ, since $g_x < 0$. Both R_a and L_a are negative, but $\omega_L > 0$ and the system is stable for $\Delta > 0$, as shown in Figs. 5(e) and 5(f).

VIII. ELECTROCHEMICAL REACTION WITH ADSORBED INTERMEDIATE

In the field of electrochemical reactions, the chemical inductor[10–13,45] and the oscillatory reactions[2,5,15,38–40,46–48] have been amply studied by impedance spectroscopy in the last few decades. Here, we summarize the properties of the reaction with an adsorbed intermediate as described by Sadkowsky.[7] The model electrocatalytic reaction consists of two elementary steps with two reagents A and C in solution and an adsorbed intermediate B_{ads},

$$A \leftrightarrow B_{ads} + n_1 e^-, \tag{28}$$

$$B_{ads} \leftrightarrow C + n_2 e^-. \tag{29}$$

Here, n_1 and n_2 are the charges transferred in each of the partial equations. The fractional concentration of adsorbed species is the slow variable, $x = \theta$. The system is characterized by the equations

$$f = n_1 v_1 + n_2 v_2, \tag{30}$$

$$g = v_1 - v_2, \tag{31}$$

where $v_1(u,\theta)$, and $v_2(u,\theta)$ are the rates of the two partial electrochemical adsorption reactions. These rates can be given a specific Butler–Volmer form.[7,48,49]

The following quantities are obtained:

$$R_b = \frac{R_I}{n_1 v_{1u} + n_2 v_{2u}}, \tag{32}$$

$$R_a = -\frac{R_I(v_{1\theta} - v_{2\theta})}{(v_{1u} - v_{2u})(n_1 v_{1\theta} + n_2 v_{2\theta})}, \tag{33}$$

$$L_a = \frac{R_I \tau_k}{(v_{1u} - v_{2u})(n_1 v_{1\theta} + n_2 v_{2\theta})}. \tag{34}$$

Hence, the characteristic frequency is

$$\omega_L = -\frac{v_{1\theta} - v_{2\theta}}{\tau_k}. \tag{35}$$

The trace of the Jacobian is

$$T_\lambda = -\frac{n_1 v_1 + n_2 v_2}{\tau_u} + \frac{v_{1\theta} - v_{2\theta}}{\tau_k}. \tag{36}$$

Galvanostatic oscillations in electrochemical systems are typically associated with a negative R_b;[6] however, Eqs. (32)–(34) show that this type of systems also allow the instability in the inductor branch with a negative ω_L.

IX. OSCILLATIONS OF A MODEL MEMRISTOR

Memristor devices can produce artificial neurons and synapses for computation algorithms based on neuron spiking.[50–56] Equivalent circuits using inductors and memristors have been used for the simulation of repetitive neuron firing.[37,57–59] Equations (1) and (2) constitute a standard model for voltage-controlled memristors,[60,61] and the associated impedance response has been discussed,[62,63] including the chemical inductor impedance.[14,64,65] Here, we derive the impedance

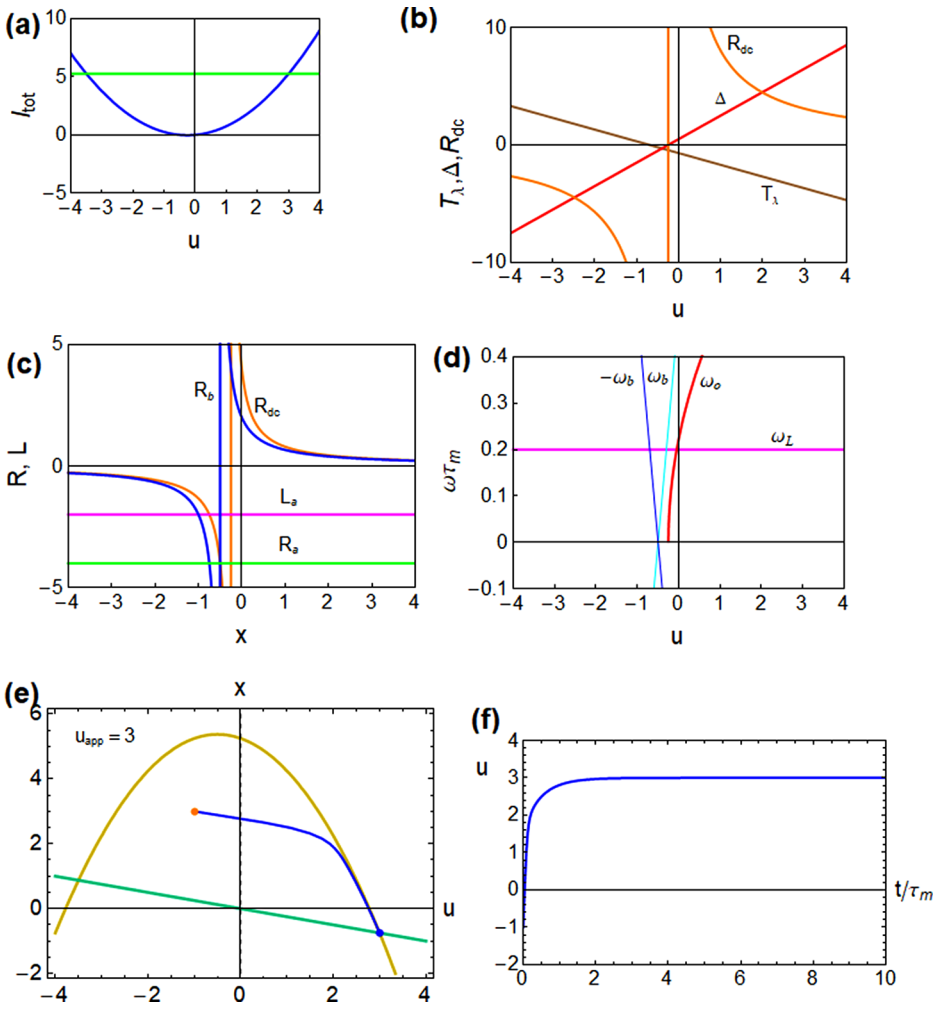

FIG. 5. Representation of a dynamical model: (a) current–voltage curve. The green line indicates the stationary point of [(e) and (f)]. (b) Stability variables. (c) Characteristic frequencies. (d) Circuit elements. (e) Nullclines and trajectory in phase space. The *f*-nullcline is the yellow line, and *g*-nullcline is the green line. The orange point is the starting condition. (d) Voltage evolution with time. Parameters $R_I = 1$, $r = -0.5$, $\beta = -2$, $a = 0.5$, $\tau_u = 10^{-1}$, and $\epsilon = 0.1$.

responses of the model of Ushakov *et al.* for a diffusive memristor in a neuromorphic circuit that shows periodic oscillations.[19]

In the model, x is the position of a nanoparticle that determines the conduction mechanism. Equations (1) and (2) adopt the following forms:

$$f = \frac{u}{\cosh\left(\frac{x}{\delta}\right)}, \tag{37}$$

$$g = F(x) - \frac{u}{u_r}. \tag{38}$$

Here, δ and u_r are material constants. The function F is defined

$$F(x) = (x-0.1)^2 - 0.001 + 8e^{-\frac{(x-0.01)^2}{0.05^2}} - \frac{8}{1.3}\left(\frac{x}{1.3}\right)^7 e^{-\left(\frac{x}{1.3}\right)^8} - 100x^{99}. \tag{39}$$

The nullclines $\dot{u} = 0$, $\dot{x} = 0$ have the expressions

$$u = R_I I_{tot} \cosh\left(\frac{x}{\delta}\right), \tag{40}$$

$$u = u_r F(x). \tag{41}$$

These forms are shown in Fig. 6(a). The steady state current–voltage is given by the intersection of nullclines

$$I_{dc}(x) = \frac{u_r}{R_I}\frac{F(x)}{\cosh\left(\frac{x}{\delta}\right)}. \tag{42}$$

It has two main branches, for $x > 0$ and $x < 0$, as shown in Fig. 6(b). We will focus on $x > 0$, which is shown separately in Fig. 6(c). The current is single valued with respect to x as shown in Fig. 6(d). Significant points are listed in Table IV. There is a saddle-node bifurcation when $F'(x) = 0$, which gives a change from one to three intercepts. This happens at $x_{01} = 0.1599$ and $x_{02} = 0.7645$.

To calculate the response to a small perturbation, we obtain the coefficients

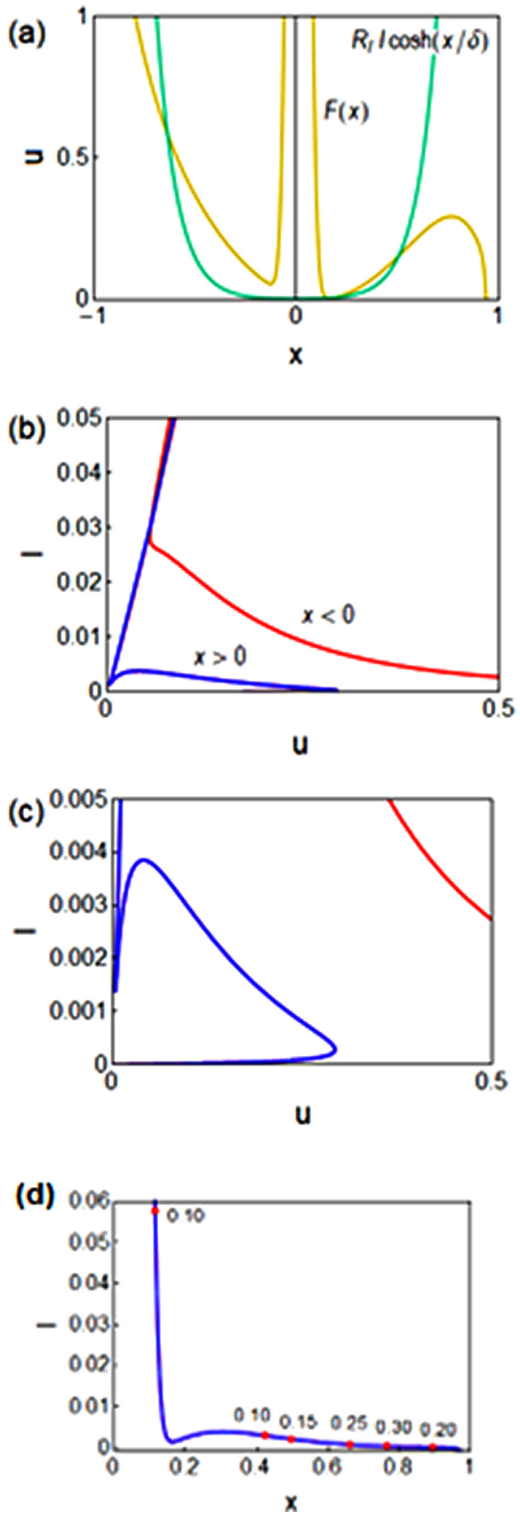

FIG. 6. (a) Representation of the nullclines for $R_I = 1$, $\delta = 0.1$, $I = 0.002$. (b) The two branches of the $I - u$ curve. (c) Enlarged view of the positive x branch. (d) Representation of $I(x)$ at different values of u as indicated.

TABLE IV. Selected points in current–voltage curve.

x	u	I_{dc}	
0.150	0.004 648	$I_1 = 0.001\,976$	
0.1590	0.003 591 1	$I_2 = 0.001\,406$	
$x_{01} = 0.1599$	0.003 591	0.001 406	$F'(x) = 0$. Minimum $u(x)$.
0.1620	0.003 617	$I_3 = 0.001\,377\,5$	
0.1623	0.003 620	0.001 377 23	Minimum $I - u$. Pass to $R_{dc} > 0$
0.186 74	0.006 546	$I_1 = 0.001\,976$	
0.3043	0.040 50	0.003 854	Maximum $I - u$ pass to $R_{dc} < 0$
0.5058	0.1554	$I_1 = 0.001\,976$	
0.562 92	0.1957	$I_2 = 0.001\,406$	
0.564 43	0.1968	0.001 392	Hopf $T_\lambda = 0$
0.566 13	0.198 023	$I_3 = 0.001\,377\,4$	
0.7499	0.2921	0.000 323 5	Hopf $T_\lambda = 0$
$x_{02} = 0.7645$	0.2930	0.000 280 4	$F'(x) = 0$. Pass to $R_{dc} > 0$

$$f_u = \frac{R_I}{R_b}, \tag{43}$$

$$f_x = -\frac{R_I}{R_\delta} u_r, \tag{44}$$

$$g_u = -\frac{1}{u_r}, \tag{45}$$

$$g_x = F'(x). \tag{46}$$

Here, the resistances are defined as follows:

$$R_b = R_I \cosh\left(\frac{x}{\delta}\right), \tag{47}$$

$$R_\delta = R_I \frac{u_r \delta}{u} \frac{\cosh^2\left(\frac{x}{\delta}\right)}{\sinh\left(\frac{x}{\delta}\right)}. \tag{48}$$

The model leads to the equivalent circuit of Fig. 1 with the circuit element values given in row 7 of Table I. The dc resistance $R_{dc} = Z(\omega = 0)$ is given by

$$R_{dc}^{-1} = \frac{1}{R_b} - \frac{1}{R_\delta F'}. \tag{49}$$

This result can be obtained also by the voltage derivative of Eq. (32). The trace and determinant are

$$T_\lambda = \frac{1}{\tau_k}\left(\epsilon F' - \frac{R_I}{R_b}\right), \tag{50}$$

$$\Delta = \frac{\varepsilon}{\cosh\left(\frac{x}{\delta}\right)}\left(\frac{F}{u_r \delta}\tanh\left(\frac{x}{\delta}\right) - F'\right) = \varepsilon R_I\left(\frac{1}{R_\delta} - \frac{F'}{R_b}\right) = -\frac{\varepsilon R_I F'}{R_{dc}}. \tag{51}$$

The analysis of stability parameters is shown in Fig. 7. In contrast to FHN, in this model R_b is positive for any x. Since $g_x = F'$, we observe in the central region of Fig. 7(a) that F' is positive and $\omega_L < 0$ for $x_{01} < x < x_{02}$ (Table IV). Here, the x variable becomes destabilizing. The positive value of g_x is due to a negative R_a, while the inductor L_a is positive. Inside this domain, there are regions with Δ either negative or positive, and in the latter, there is a region in which $T_\lambda > 0$. Note in Fig. 7(b) the condition (25) for the Hopf bifurcation, by the intercept of ω_L and $-\omega_b$, that determines the set of points in which $T_\lambda > 0$.

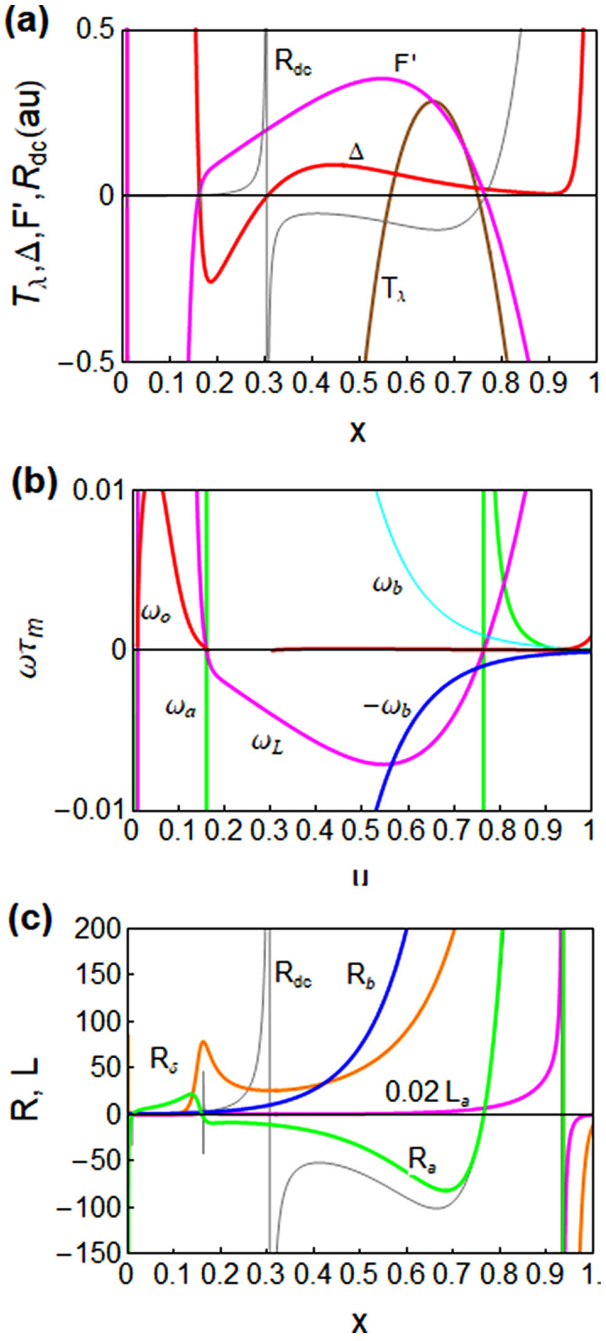

FIG. 7. (a) Stability variables. Values $\Delta = 0$ are at $x = 0.1623$, 0.3043; $T_\lambda = 0$ at $x = 0.5644$, 0.7499. (b) Characteristic frequencies. (c) Circuit elements. Parameters $R_l = 1$, $\delta = 0.1$, $\tau_u = 10^{-2}$, $\epsilon = 0.01$. $R_{dc} < 0$ at $0.1599 < x < 0.1623$ and at $0.3043 < x < 0.7645$.

Figure 8 presents the dynamical evolution for selected values of the fixed point x_1. In the domain where $T_\lambda > 0$ limit cycle oscillations occur. This happens even though the dc resistance is negative, since the determinant is positive. At $x_{03} = 0.935$, both the inductor L_a and R_a become negative, but this regime with $\omega_L > 0$ does not introduce instabilities as discussed in Sec. VII.

The different impedance spectra for the stationary x_1 values are shown in Fig. 9. The most remarkable result is in Fig. 9(f) for the region of limit cycle oscillations. The impedance contains a negative resistance at finite frequencies, but the dc resistance is negative and the spectrum is different compared to Fig. 4(j).

X. OSCILLATIONS IN HODGKIN–HUXLEY MODEL

The Hodgkin–Huxley (HH) dynamical model for the squid giant axon membrane[66] is a central piece of the description of neuronal behavior. Impedance and bifurcation of the Hodgkin–Huxley model have been analyzed by Chua and co-workers.[67,68] Here, we use the results of a previous calculation[53] to show the role of different elements in the small perturbation equivalent circuit, including negative inductors.

The HH model is composed of four differential equations. One has the form of Eq. (1) and three additional equations that describe the slow variable dynamics of two ion channels.[1] This model lays outside the above classification for two-dimensional systems. However, we find that the structure described in the previous 2D approach is nested in the higher order HH model so that our discussion is useful for the interpretation of the neuron spiking.

For example, the internal state variables for the sodium channel obey the following equations:

$$\frac{dm}{dt} = \alpha_m(V)(1-m) - \beta_m(V)m, \tag{52}$$

$$\frac{dh}{dt} = \alpha_h(V)(1-h) - \beta_h(V)h. \tag{53}$$

The parameters are defined in Ref. 53. These two equations have the standard form of the chemical inductor structure, Eq. (2), and they lead to the equivalent circuit elements,[53]

$$R_m(\overline{V}_M) = \frac{R_{Na0}}{3\overline{m}^2\overline{h}(\overline{V}_M - V_{Na})\tau_m\left[\frac{\partial\overline{\alpha}_m}{\partial V_M}(1-\overline{m}) - \frac{\partial\overline{\beta}_m}{\partial V_M}\overline{m}\right]}, \tag{54}$$

$$L_m(\overline{V}_M) = R_m\tau_m, \tag{55}$$

$$R_h(\overline{V}_M) = \frac{R_{Na0}}{\overline{m}^3(\overline{V}_M - V_{Na})\tau_h\left[\frac{\partial\overline{\alpha}_h}{\partial V_M}(1-\overline{h}) - \frac{\partial\overline{\beta}_h}{\partial V_M}\overline{h}\right]}, \tag{56}$$

$$L_h(\overline{V}_M) = R_h\tau_h, \tag{57}$$

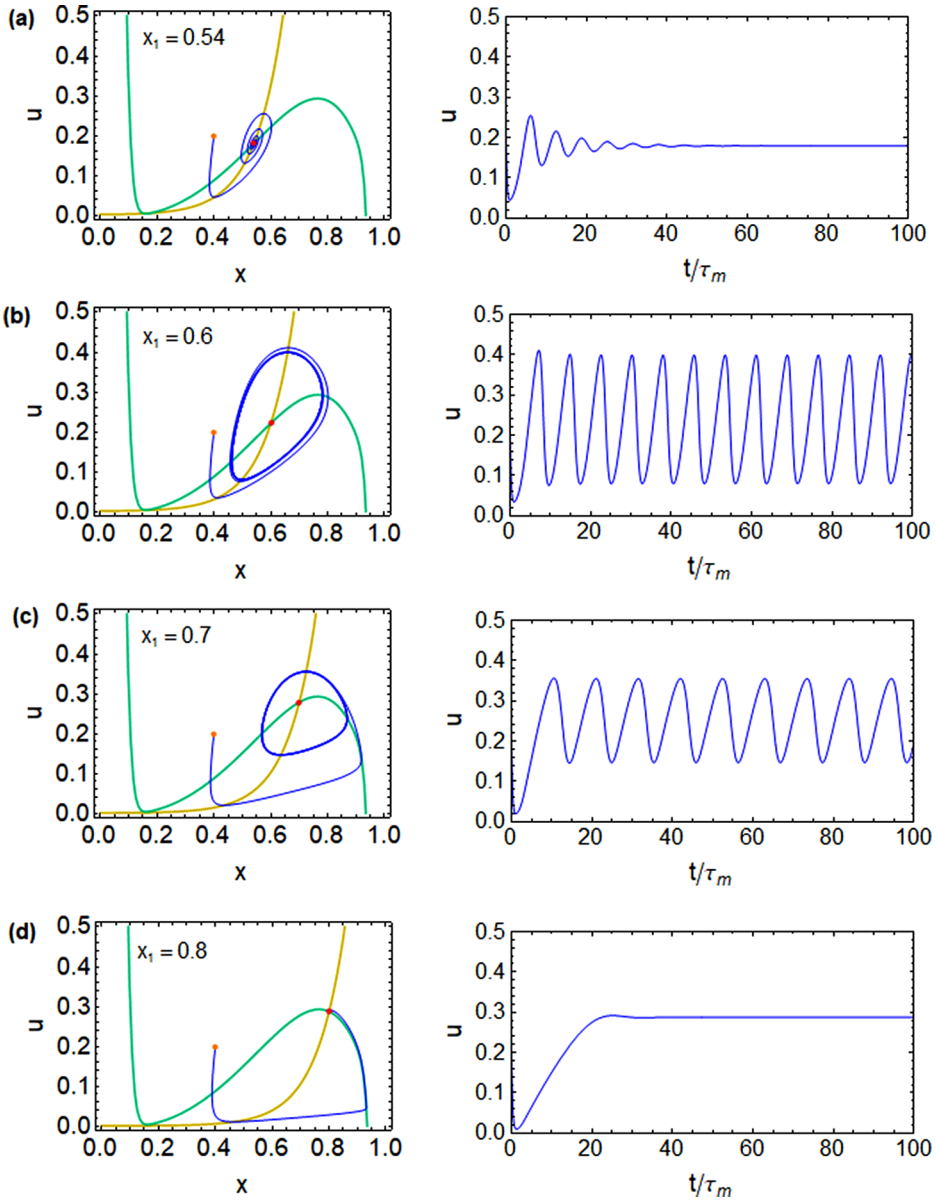

FIG. 8. Trajectories in phase plane and voltage evolution with time of a model memristor for different values of the fixed point x_1 indicted by a red point. The orange point is the starting condition.

where the relaxation time constants τ_i of the activation-gate variables are defined as follows:

$$\tau_i = \frac{1}{\alpha_i + \beta_i}. \tag{58}$$

The HH membrane model was originally depicted using variable resistances as indicated in Fig. 10(a).[66] The small perturbation equivalent circuit of the HH model is shown in Fig. 10(b).[53] It is obviously a multiple combination of the essential structure of Fig. 1. Figure 10(b) contains one chemical inductor for the potassium channel (blue), and a double chemical inductor subcircuit for the sodium channel (red). The presence of the inductor in the axon membrane impedance was well recognized by Cole and Baker much earlier than the development of the HH model.[14,69,70]

Following the modern convention,[71,72] we consider a resting potential of the neuron of $V_r = -65\,\text{mV}$ at a temperature of $T = 6.3\,^{\circ}\text{C}$.[66] The neuron oscillation occurs in a narrow voltage range between $V_M = -42.99\,\text{mV}$ and $V_M = -60.25\,\text{mV}$. In Fig. 11, we show the full impedance spectra in a set of selected voltages. Clearly, the oscillating region of voltages is characterized by the impedance pattern with a negative finite resistance, shown in Fig. 11(c). This is associated with a Hopf bifurcation as explained in Fig. 4(j).

In Fig. 12, we show the impedances of the sodium channel components. We observe that there are both a positive inductor, h, and a

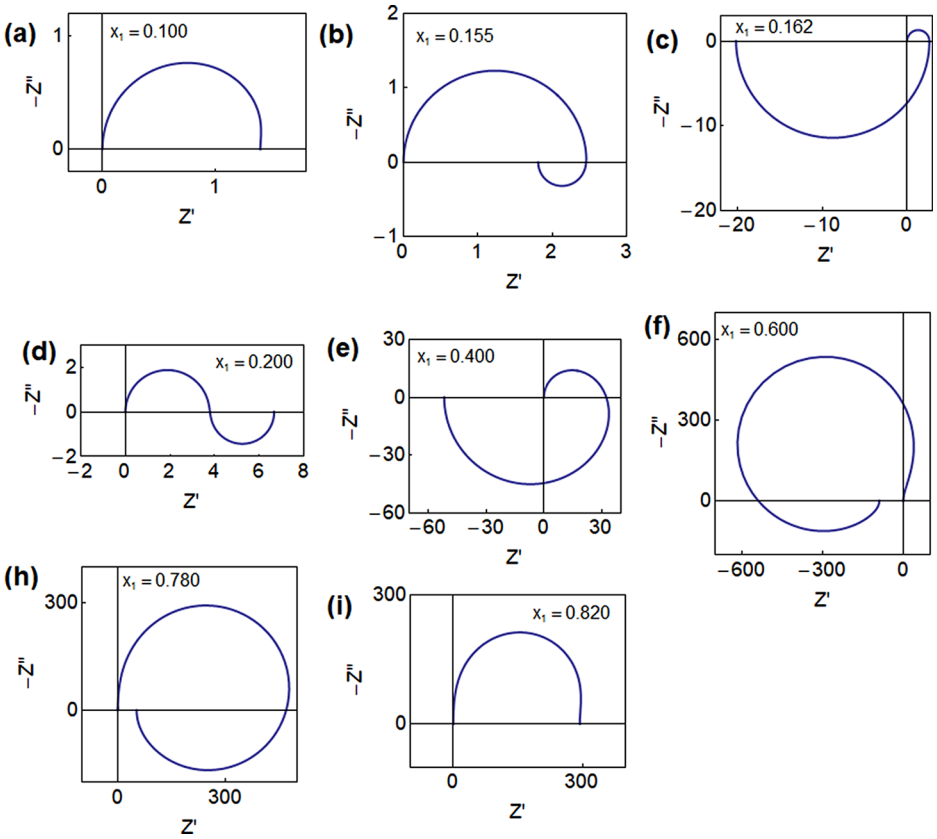

FIG. 9. Evolution of impedance spectra at different values of the fixed point x_1.

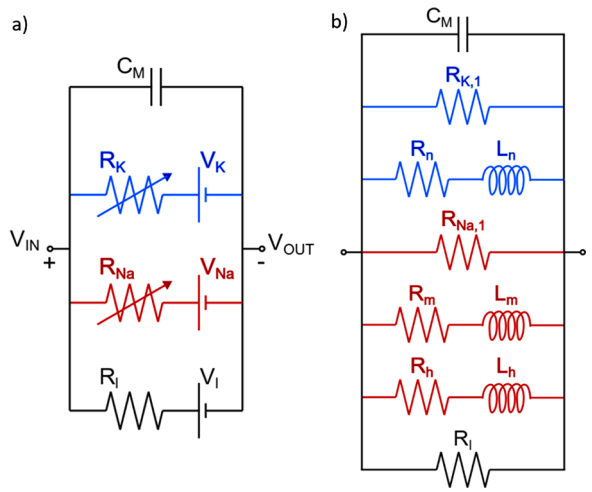

FIG. 10. (a) Hodgkin–Huxley electrical model for the squid giant axon membrane consisting of variable resistances in the ion channels as defined in the original publication. (b) Equivalent circuit for the Hodgkin–Huxley model for small ac voltage perturbations. The potassium channel components are indicated in blue, and the sodium elements in red.[53]

negative inductor, m. However, the resistance R_m accompanying the negative inductor is also negative, hence $\tau_L > 0$ and the inductor line is stable.

On the other hand, the total resistance of the sodium channel between -40 and -60 mV is negative as observed in the impedance spectra of Fig. 13(a). We conclude that the oscillations in the HH axon model are not due to a negative inductor component but to the coupling of the negative resistance of the sodium channel with the inductor elements in the sodium and potassium channels.

XI. CONCLUSION

A general analysis of 2D nonlinear oscillating systems shows that the signs of the derivatives of the constituent functions translate into a classification of signs of the equivalent circuit elements. In turn, these elements determine the stability or oscillating conditions according to a set of characteristic frequencies formed by the products of the circuit elements. When viewed by a small perturbation in the frequency domain, the essential structure of the models is composed of a conducting line, an inductor line, and a parallel capacitance. The system can be destabilized by a negative resistance in either the conducting line or the inductor branch. When the system contains negative elements in the inductor branch, the sign of the dc resistance and the

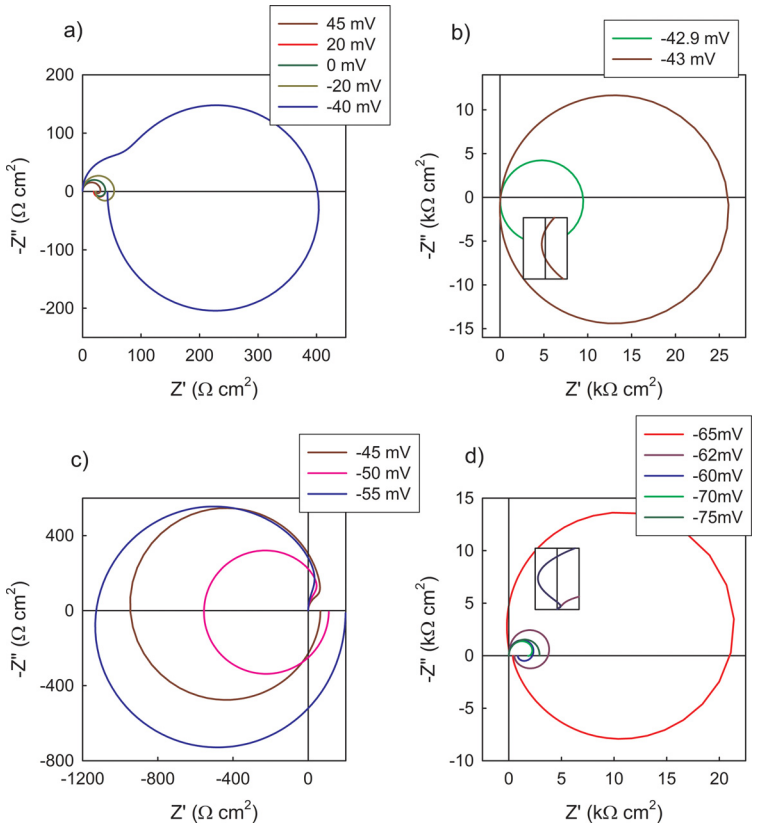

FIG. 11. Impedance complex plane plots for voltages (a) above the upper limit of the negative impedance region, (b) around the upper limit $V_M = -42.99$ mV, (c) in the negative impedance region and (d) around the lower limit $V_M = -60.25$ mV.

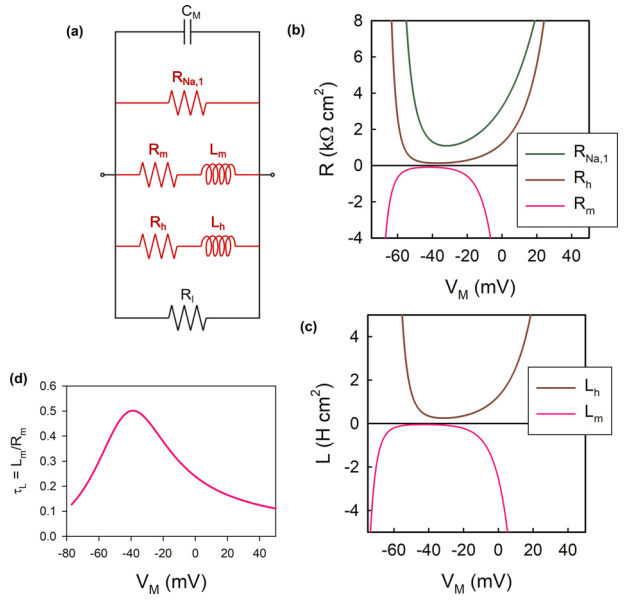

FIG. 12. Impedance details of the Na channel. (a) EC used of the Na channel. (b) and (c) Values of the resistances and inductors for the range of membrane voltages, respectively. (d) Inductor characteristic time.

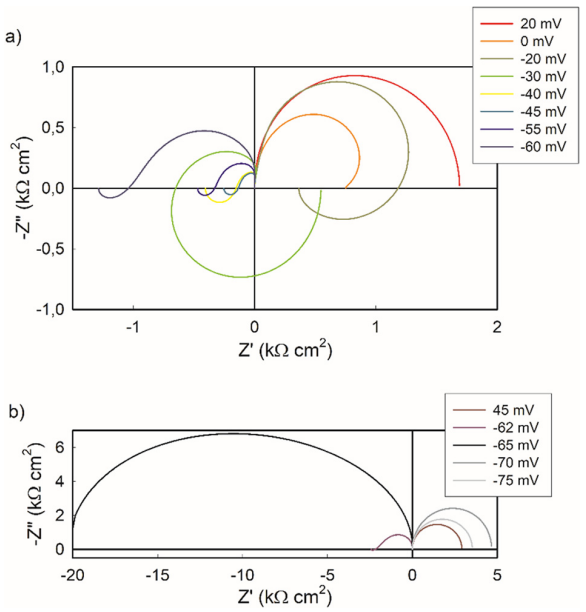

FIG. 13. Impedance complex plane plots for the sodium channel EC. (a) is for spectra with smaller impedance values and (b) is for spectra with bigger impedance values.

sign of the determinant can be reversed. The presence of a negative inductor has been found in many systems, including the classical Hodgkin–Huxley neuron model. However, the negative inductor *per se* does not indicate instability.

ACKNOWLEDGMENTS

We thank Generalitat Valenciana for the financial support by a Prometeo Grant (No. PROMETEU/2020/028).

AUTHOR DECLARATIONS

Conflict of Interest

The author have no conflicts to disclose.

Author Contributions

Juan Bisquert: Conceptualization (lead); Writing – original draft (lead).

DATA AVAILABILITY

Data sharing is not applicable to this article as no new data were created or analyzed in this study.

REFERENCES

[1]E. M. Izhikevich, *Dynamical Systems in Neuroscience* (MIT Press, 2007).
[2]M. T. M. Koper, "Non-linear phenomena in electrochemical systems," J. Chem. Soc., Faraday Trans. **94**, 1369–1378 (1998).
[3]Z. Luo, Y. Bo, S. M. Sadaf, and X. Liu, "Van der Pol oscillator based on NbO_2 volatile memristor: A simulation analysis," J. Appl. Phys. **131**, 054501 (2022).
[4]V. Vivier and M. E. Orazem, "Impedance analysis of electrochemical systems," Chem. Rev. **122**, 11131–11168 (2022).
[5]M. T. M. Koper, "Oscillations and complex dynamical bifurcations in electrochemical systems," Adv. Chem. Phys. **92**, 161 (1996).
[6]M. Keddam, H. Takenouti, and N. Yu, "Transpassive dissolution of Ni in acidic sulfate media: A kinetic model," J. Electrochem. Soc. **132**, 2561–2566 (1985).
[7]A. Sadkowski, "Small signal local analysis of electrocataytical reaction. Pole-zero approach," J. Electroanal. Chem. **465**, 119–128 (1999).
[8]A. Sadkowski, "On specific properties of electrochemical immittance close to discontinuity points," Electrochim. Acta **49**, 2653–2659 (2004).
[9]S. A. Sarles, J. P. Wright, and J.-S. Pei, "Equilibrium analysis of Mott memristor reveals criterion for negative differential resistance," Appl. Phys. Lett. **118**, 223505 (2021).
[10]I. Elpelboin and M. Keddam, "Faradaic impedances: Diffusion impedance and reaction impedance," J. Electrochem. Soc. **117**, 1052 (1970).
[11]C.-N. Cao, "On the impedance plane displays for irreversible electrode reactions based on the stability conditions of the steady-state. I. One state variable besides electrode potential," Electrochim. Acta **35**, 831–836 (1990).
[12]J. P. Diard, P. Landaud, B. Le Gorrec, and C. Montella, "Calculation, simulation and interpretation of electrochemical impedance. II. Interpretation of Volmer-Heyrovsky impedance diagrams," J. Electroanal. Chem. Interfacial Electrochem. **255**, 1–20 (1988).
[13]J. P. Diard, B. Le Gorrec, and C. Montella, "Calculation, simulation and interpretation of electrochemical impedances. III. Conditions for observation of low frequency inductive diagrams for a two-step electron transfer reaction with an adsorbed intermediate species," J. Electroanal. Chem. **326**, 13–36 (1992).
[14]J. Bisquert and A. Guerrero, "Chemical inductor," J. Am. Chem. Soc. **144**, 5996–6009 (2022).
[15]P. Strasser, M. Eiswirth, and M. T. M. Koper, "Mechanistic classification of electrochemical oscillators—An operational experimental strategy," J. Electroanal. Chem. **478**, 50–66 (1999).
[16]E. M. Izhikevich, "Simple model of spiking neurons," IEEE Trans. Neural Networks **14**, 1569–1572 (2003).
[17]E. Schöll, *Nonequilibrium Phase Transitions in Semiconductors* (Springer-Verlag, 1987).
[18]J. Bisquert, "Hopf bifurcations in electrochemical, neuronal, and semiconductor systems analysis by impedance spectroscopy," Appl. Phys. Rev. **9**, 011318 (2022).
[19]Y. Ushakov, A. Akther, P. Borisov, D. Pattnaik, S. Savel'ev, and A. G. Balanov, "Deterministic mechanisms of spiking in diffusive memristors," Chaos Solitons Fractals **149**, 110997 (2021).
[20]I. K. Schuller, A. Frano, R. C. Dynes, A. Hoffmann, B. Noheda, C. Schuman, A. Sebastian, and J. Shen, "Neuromorphic computing: Challenges from quantum materials to emergent connectivity," Appl. Phys. Lett. **120**, 140401 (2022).
[21]Y. Tuchman, T. N. Mangoma, P. Gkoupidenis, Y. van de Burgt, R. A. John, N. Mathews, S. E. Shaheen, R. Daly, G. G. Malliaras, and A. Salleo, "Organic neuromorphic devices: Past, present, and future challenges," MRS Bull. **45**, 619–630 (2020).
[22]Y. van de Burgt and P. Gkoupidenis, "Organic materials and devices for brain-inspired computing: From artificial implementation to biophysical realism," MRS Bull. **45**, 631–640 (2020).
[23]M. Javad, M. Hossein, E. Donati, T. Yokota, S. Lee, G. Indiveri, T. Someya, and R. A. Nawrocki, "Organic electronics Axon-Hillock neuromorphic circuit: Towards biologically compatible, and physically flexible, integrate-and-fire spiking neural networks," J. Phys. D: Appl. Phys. **54**, 104004 (2021).
[24]R. A. John, N. Tiwari, M. I. B. Patdillah, M. R. Kulkarni, N. Tiwari, J. Basu, S. K. Bose, A. Ankit, C. J. Yu, A. Nirmal, S. K. Vishwanath, C. Bartolozzi, A. Basu, and N. Mathews, "Self healable neuromorphic memtransistor elements for decentralized sensory signal processing in robotics," Nat. Commun. **11**, 4030 (2020).
[25]J. Bisquert and A. Guerrero, "Dynamic instability and time domain response of a model halide perovskite memristor for artificial neurons," J. Phys. Chem. Lett. **13**, 3789–3795 (2022).
[26]W. Gerstner, W. M. Kistler, R. Naud, and L. Paninski, *Neuronal Dynamics: From Single Neurons to Networks and Models of Cognition* (Cambridge University Press, 2014).
[27]A. Guerrero, J. Bisquert, and G. Garcia-Belmonte, "Impedance spectroscopy of metal halide perovskite solar cells from the perspective of equivalent circuits," Chem. Rev. **121**, 14430–14484 (2021).
[28]A. Lasia, *Electrochemical Impedance Spectroscopy and its Applications* (Springer, 2014).
[29]D. E. Root and B. Hughes, "Principles of nonlinear active device modeling for circuit simulation," in Proceedings of the 32nd ARFTG Conference Digest (1988).
[30]J. C. Pedro, D. E. Root, J. Xu, and L. C. Nunes, *Nonlinear Circuit Simulation and Modeling: Fundamentals for Microwave Design* (Cambrige, UP, 2018).
[31]E. Hernández-Balaguera and J. Bisquert, "Negative transient spikes in halide perovskites," ACS Energy Lett. **2022**, 2602–2610.
[32]E. Ghahremanirad, A. Bou, S. Olyaee, and J. Bisquert, "Inductive loop in the impedance response of perovskite solar cells explained by surface polarization model," J. Phys. Chem. Lett. **8**, 1402–1406 (2017).
[33]C. Gonzales, A. Guerrero, and J. Bisquert, "Transition from capacitive to inductive hysteresis: A neuron-style model to correlate I-V curves to impedances of metal halide perovskites," J. Phys. Chem. C **126**, 13560–13578 (2022).
[34]C. Rocşoreanu, A. Georgescu, and N. Giurgiţeanu, *The FitzHugh-Nagumo Model: Bifurcation and Dynamics* (Kluwer Academic Publishers, 2000).
[35]T. Kostova, R. Ravindran, and M. Schonbek, "Fitzhugh–Nagumo revisited: Types of bifurcations, periodical forcing and stability regions by a Lyapunov functional," Int. J. Bifurcation Chaos **14**, 913–925 (2004).
[36]D. Armbruster, "The (almost) complete dynamics of the Fitzhugh Nagumo equations," Nonlinear Dyn. **2**, 89–102 (1997).
[37]J. Bisquert, "A frequency domain analysis of excitability and bifurcations of Fitzhugh-Nagumo neuron model," J. Phys. Chem. Lett. **12**, 11005–11013 (2021).
[38]F. Berthier, J.-P. Diard, and C. Montella, "Hopf bifurcation and sign of the transfer resistance," Electrochim. Acta **44**, 2397 (1999).

[39]V. V. Pototskaya, O. I. Gichan, A. A. Omelchuk, and S. V. Volkov, "Specific features of the behavior of an electrochemical system in the case of the Hopf instability for a spherical electrode," Russ. J. Electrochem. **44**, 594–601 (2008).
[40]F. Berthier, J.-P. L. Diard, B. Gorrec, and C. Montella, "Discontinuous immittance due to a saddle node bifurcation. I. 1-, 2- and 3-part immittance diagrams," J. Electroanal. Chem. **458**, 231–240 (1998).
[41]J. Guckenheimer, M. Myers, and B. Sturmfels, "Computing Hopf Bifurcations. I," SIAM J. Sci. Comput. **34**, 1–21 (1997).
[42]J. Guckenheimer and M. Myers, "Computing Hopf Bifurcations. II. Three examples from neurophysiology," SIAM J. Sci. Comput. **17**, 1275–1301 (1996).
[43]K. S. Cole and R. F. Baker, "Longitudinal impedance of the squid giant axon," J. Gen. Physiol. **24**, 771–788 (1941).
[44]I. Mora-Seró, J. Bisquert, F. Fabregat-Santiago, G. Garcia-Belmonte, G. Zoppi, K. Durose, Y. Y. Proskuryakov, I. Oja, A. Belaidi, T. Dittrich, R. Tena-Zaera, A. Katty, C. Lévy-Clement, V. Barrioz, and S. J. C. Irvine, "Implications of the negative capacitance observed at forward bias in nanocomposite and polycrystalline solar cells," Nano Lett. **6**, 640–650 (2006).
[45]H. Göhr and C.-A. Schiller, "Faraday-Impedanz als Verknüpfung von Impedanzelementen," Z. Phys. Chem. **148**, 105–124 (1986).
[46]K. Krischer, "Nonlinear dynamics in electrochemical systems," in *Advances in Electrochemical Science and Engineering*, edited by R. C. Alkire and D. M. Kolb (Wiley, 2002), pp. 89–208.
[47]M. Orlic, *Self-Organization in Electrochemical Systems I* (Springer, 2012).
[48]M. Naito, N. Tanaka, and H. Okamoto, "General relationship between complex impedance and linear stability in electrochemical systems," J. Chem. Phys. **111**, 9908–9917 (1999).
[49]A. Sadkowski, "On some dynamic peculiarities of the charge transfer with adsorption and attractive interactions," Electrochim. Acta **49**, 2259 (2004).
[50]K. Kang, W. Hu, and X. Tang, "Halide perovskites for resistive switching memory," J. Phys. Chem. Lett. **12**, 11673–11682 (2021).
[51]K. J. Kwak, D. E. Lee, S. J. Kim, and H. W. Jang, "Halide perovskites for memristive data storage and artificial synapses," J. Phys. Chem. Lett. **12**, 8999–9010 (2021).
[52]H. J. Gogoi, K. Bajpai, A. T. Mallajosyula, and A. Solanki, "Advances in flexible memristors with hybrid perovskites," J. Phys. Chem. Lett. **12**, 8798–8825 (2021).
[53]A. Bou and J. Bisquert, "Impedance spectroscopy dynamics of biological neural elements: From memristors to neurons and synapses," J. Phys. Chem. B **125**, 9934–9949 (2021).
[54]M. Rahimi Azghadi, Y.-C. Chen, J. K. Eshraghian, J. Chen, C.-Y. Lin, A. Amirsoleimani, A. Mehonic, A. J. Kenyon, B. Fowler, J. C. Lee, and Y.-F. Chang, "Complementary metal-oxide semiconductor and memristive hardware for neuromorphic computing," Adv. Intell. Syst. **2**, 1900189 (2020).
[55]A. Mehonic and A. J. Kenyon, "Emulating the electrical activity of the neuron using a silicon oxide RRAM cell," Front. Neurosci. **10**, 57 (2016).
[56]J. Gong, H. Wei, Y. Ni, S. Zhang, Y. Du, and W. Xu, "Methylammonium halide-doped perovskite artificial synapse for light-assisted environmental perception and learning," Mater. Today Phys. **21**, 100540 (2021).
[57]G. Innocenti, M. Di Marco, A. Tesi, and M. Forti, "Memristor circuits for simulating neuron spiking and burst phenomena," Front. Neurosci. **15**, 681035 (2021).
[58]M. D. Marco, M. Forti, G. Innocenti, A. Tesi, and F. Corinto, "Targeting multistable dynamics in a second-order memristor circuit," in Proceedings of the IEEE International Symposium on Circuits and Systems (ISCAS) (2020).
[59]M. D. Marco, M. Forti, G. Innocenti, and A. Tesi, "Transient control in targeting multistable dynamics of a memristor circuit," in Proceedings of the IEEE International Symposium on Circuits and Systems (ISCAS) (2021).
[60]L. Chua, "Memristor, Hodgkin–Huxley, and edge of chaos," Nanotechnology **24**, 383001 (2013).
[61]Y. V. Pershin and M. Di Ventra, "Memory effects in complex materials and nanoscale systems," Adv. Phys. **60**, 145–227 (2011).
[62]A. Ascoli, A. S. Demirkol, R. Tetzlaff, S. Slesazeck, T. Mikolajick, and L. O. Chua, "On local activity and edge of chaos in a NaMLab memristor," Front. Neurosc. **15**, 651452 (2021).
[63]A. Ascoli, A. S. Demirkol, R. Tetzlaff, and L. Chua, "Edge of chaos theory resolves smale paradox," IEEE Trans. Circuits Syst. I: Regul. Pap. **69**, 1252–1265 (2022).
[64]M. Berruet, J. C. Pérez-Martínez, B. Romero, C. Gonzales, A. M. Al-Mayouf, A. Guerrero, and J. Bisquert, "Physical model for the current-voltage hysteresis and impedance of halide perovskite memristors," ACS Energy Lett. **7**, 1214–1222 (2022).
[65]L. Munoz-Diaz, A. J. Rosa, A. Bou, R. S. Sanchez, B. Romero, R. A. John, M. V. Kovalenko, A. Guerrero, and J. Bisquert, "Inductive and capacitive hysteresis of halide perovskite solar cells and memristors under illumination," Front. Energy Res. **10**, 914115 (2022).
[66]A. L. Hodgkin and A. F. Huxley, "A quantitative description of membrane current and its application to conduction and excitation in nerve," J. Physiol. **117**, 500–544 (1952).
[67]L. Chua, V. Sbitnev, and H. Kim, "Neurons are poised near the edge of chaos," Int. J. Bifurcation Chaos **22**, 1250098 (2012).
[68]L. Chua, V. Sbitnev, and H. Kim, "Hodgkin–Huxley axon is made of memristors," Int. J. Bifurcation Chaos **22**, 1230011 (2012).
[69]K. S. Cole, "Rectification and inductance in the squid giant axon," J. Gen. Physiol. **25**, 29–51 (1941).
[70]K. S. Cole, *Membranes, Ions and Impulses: A Chapter of Classical Biophysics* (University of California Press, 1968).
[71]J. Malmivuo and R. Plonsey, *Bioelectromagnetism: Principles and Applications of Bioelectric and Biomagnetic Fields* (Oxford University Press, 1995).
[72]E. R. Kandel, *Principles of Neural Science* (McGraw-Hill, 2013).